The Astrophysical Journal, 932:119 (8pp), 2022 June 20 https://doi.org/10.3847/1538-4357/ac6ddd

Formation and Abundance of Late-forming Primordial Black Holes as Dark Matter

Amlan Chakraborty[1], Prolay K Chanda[2], Kanhaiya Lal Pandey[1], and Subinoy Das[1]
[1] Indian Institute of Astrophysics, Bengaluru, Karnataka 560034, India; amlan.chakraborty@iiap.res.in, kanhaiya.pandey@iiap.res.in,subinoy@iiap.res.in
[2] Department of Physics, University of Illinois at Chicago, Chicago, IL 60607, USA; pchand31@uic.edu
Received 2022 April 27; accepted 2022 May 5; published 2022 June 23

Abstract

We propose a novel mechanism where primordial black hole (PBH) dark matter is formed much later in the history of the universe, between the epochs of Big Bang nucleosynthesis and cosmic microwave background photon decoupling. In our setup, one does not need to modify the scale-invariant inflationary power spectra; instead, a late-phase transition in a strongly interacting fermion–scalar fluid (which occurs naturally around redshift $10^6 \leqslant z_T \leqslant 10^8$) creates an instability in the density perturbation as the sound speed turns imaginary. As a result, the dark matter perturbation grows exponentially in sub-Compton scales. This follows the immediate formation of an early dense dark matter halo, which finally evolves into PBHs due to cooling through scalar radiation. We calculate the variance of the density perturbations and the PBH fractional abundances $f(M)$ by using a nonmonochromatic mass function. We find that the peak of our PBH mass function lies between 10^{-16} and 10^{-14} solar mass for $z_T \simeq 10^6$, and thus that it can constitute the entire dark matter of the universe. In PBH formation, one would expect a temporary phase where an attractive scalar balances the Fermi pressure. We numerically confirm that such a state indeed exists, and we find the radius and density profile of the temporary static structure of the dark matter halo, which finally evolves into PBHs due to cooling through scalar radiation.

Unified Astronomy Thesaurus concepts: Dark matter (353); Primordial black holes (1292); Early universe (435); Cosmology (343)

1. Introduction

Despite decades of searching, the exact nature of dark matter (DM) is still a mystery. The fact that no DM particles have been observed by direct, indirect, or collider searches casts doubt on the assumption that DM is just a weakly interactive massive particle (WIMP) motivated by electroweak-scale physics. Once we start to explore possible DM candidates beyond WIMPs, primordial black holes (PBHs) are one of the strongest and most well-studied candidates. Generally, in most of the models of PBHs, they are formed deep in a radiation-dominated era, via the collapse of large-density perturbations (Zel'dovich & Novikov 1967; Hawking 1971). Though PBHs are simple and well-motivated DM candidates, the present PBH DM density is subject to stringent constraints from various observational and theoretical studies. In principle, at the time of their generation, PBHs could have masses starting from the Planck mass (10^{-5} g) to stupendously large masses, such as $\sim 10^{17} M_{\odot}$, the horizon mass at the time of matter–radiation equality (Carr et al. 2021b). On a cosmological scale, PBH DM would behave almost like dark particle matter; however, depending on its mass, at galactic and smaller scales, it can have characteristic observable consequences. PBHs can also have implications in early black hole seeding, and in the formation of the first stars and galaxies accretion onto massive-enough PBHs can account for the detected X-ray and infrared backgrounds and their cross correlation (Cappelluti et al. 2022 and references therein). Although low-mass PBHs are expected to evaporate quickly, via Hawking radiation, those with an initial mass $\gtrsim 10^{15}$ g have a lifetime longer than the age of the universe (Hawking 1974, 1975).

There have been extensive efforts to search for PBHs using various observations. These include observations of the extra-galactic γ-ray background, gravitational microlensing experiments (e.g., OGLE-I–IV, using Kepler objects, and Eridanus II star clusters), cosmic microwave background (CMB) experiments, dynamical constraints, and accretion constraints (Laha 2019; Laha et al. 2020; Dasgupta et al. 2020; Carr & Kühnel 2020; Carr et al. 2021a, and references therein). More recently, gravitational-wave astronomy has opened up a new avenue for the search for PBHs, through the gravitational waves that are either generated by their coalescence or associated with their generation (Bird et al. 2016; Sasaki et al. 2016, 2018; Kapadia et al. 2020, 2021; Hütsi et al. 2021, and references therein). Figure 10 in Carr et al. (2021a) gives a nice overview of the current status of the PBH abundance constraints over all the possible mass ranges. From the figure, one can find that the potential allowed mass range over which PBHs can still make up the entire DM is 10^{17}–10^{24} g (10^{-16} –$10^{-10} M_{\odot}$).

PBHs are generally produced from the collapse of inhomogeneities in the early universe, unlike stellar black holes, which form from the collapse of a star. To create such extreme inhomogeneity in a very early epoch, one generally requires the modification of inflationary power spectra (Carr & Lidsey 1993; Ivanov et al. 1994; Ashoorioon et al. 2018; Sasaki et al. 2018; Bhattacharya et al. 2021) in the early universe, where the model permits a peak at a very small length scale in the primordial power spectra (García-Bellido et al. 1996; Clesse & García-Bellido 2015; Kannike et al. 2017; García-Bellido & Ruiz Morales 2017; Franciolini et al. 2018; Ezquiaga et al. 2018; Ballesteros & Taoso 2018; Pi et al. 2018; Ashoorioon et al. 2021). This implies the density contrast to be very high at those scales, which gives a perfect environment for the formation of PBHs when those modes enter the horizon.

An alternative route is to maintain the success of the simple inflationary model with scale-invariant power spectra by keeping it as it is, but creating a high subhorizon-scale density contrast with some phase transitions that naturally take place as the universe cools down. For example, QCD PBHs are formed due to the temporary drop in the pressure around the epoch of the QCD phase transition (Jedamzik 1997; Widerin & Schmid 1998; Jedamzik 1998; Hindmarsh & Philipsen 2005; Byrnes et al. 2018). However,

since the QCD PBHs will have masses of the order $\sim$0.1–10 $M_\odot$, they cannot account for all the DM, given the current constraints on $f(M)$ for these masses (see Figure 4). Other first-order phase transitions driven by bubble nucleation or bubble collision can also create PBHs (Crawford & Schramm 1982; Hawking et al. 1982; Kodama et al. 1982; La & Steinhardt 1989; Moss 1994; Konoplich et al. 1998; Konoplich et al. 1999 ; Kusenko et al. 2020; Gross et al. 2021; Baker et al. 2021; Kawana & Xie 2022). The existence of an attractive long-range fifth force (Das et al. 2021) or scalar field fragmentation (Cotner & Kusenko 2017a; Cotner & Kusenko 2017b; Cotner et al. 2018; Cotner et al. 2019) can also lead to PBH DM formation in the pre–Big Bang nucleosynthesis (BBN) era. Once PBHs form through the above processes, the PBH mass is typically of the order of the horizon size at the formation epoch. Thus, knowing the formation epoch more or less fixes the PBH mass. If the PBHs form during a radiation-dominated era, the PBH mass, $M_{\rm BH}$, differs from the horizon mass, $M_{\rm H}$, by only a factor of unity $\gamma \lesssim 1$ (Carr et al. 2021a):

$$M_{\rm BH} = \gamma M_{\rm H} = \frac{\gamma c^3 t}{G} \approx 2.03 \times 10^5 \gamma \left(\frac{t}{1\ {\rm s}}\right) M_\odot. \tag{1}$$

In this work, however, we break this simple relation between PBH mass and formation redshift by introducing a new scale to the formation process. The main goal here is to form PBHs at a later epoch (between the BBN and CMB decoupling epochs), but with the PBH masses being much less than the horizon mass at the time of formation. In standard Λ cold dark matter (CDM) cosmology, it is not possible to form PBHs during this epoch, as gravity is not strong enough to overcome radiation pressure. But the presence of a new additional force stronger than gravity can alter the story (Savastano et al. 2019; Das et al. 2021). For example, it was recently pointed out (Savastano et al. 2019) that an early dense DM halo can form deep in a radiation-dominated era when an attractive scalar force makes the DM perturbation grow much faster $\delta \sim a^p$ than standard logarithm growth. In a follow-up work on this (Flores & Kusenko 2021a), it was further demonstrated that these early halos could lose energy through scalar radiation, and could indeed form PBHs as viable DM candidates.

Here, we propose a scenario where the growth rate of the primordial inhomogeneities of a fermionic particle coupled with a scalar field can grow much faster even than polynomial. We show that exponential growth is well possible in a scalar–fermion interaction (Gogoi et al. 2021). This exponential growth occurs when our keV mass fermionic particle turns nonrelativistic, around $z_T \sim 10^6$, and the sound speed of the DM perturbation turns imaginary (Afshordi et al. 2005). We derive the matter power spectrum for the abovementioned exponential growth scenario and do a detailed calculation of the PBH mass function in this scenario, using the scaling relation for the critical gravitational collapse of a massless scalar field given by Choptuik (1993) and the Press–Schechter formalism (Press & Schechter 1974). We find that for $z_T \simeq 10^6$, the peak of the PBH mass function lies between 10^{-15} and $10^{-12} M_\odot$, and therefore it can account for almost the entire DM in the universe ($f(M) \simeq 1$), given the current constraints on the PBH abundances.

The plan of the paper is as follows. We describe the growth of the density perturbation of the fermion–scalar fluid in Section 2. In Section 3, we numerically solve for the static structure of the primordial halos. Section 4 provides the adopted formalism for the derivation of the mass function for late-forming PBHs, followed by the main numerical results. In Section 5, we summarize the main findings and offer future perspectives.

2. Late-forming PBHs: The Mechanism

This paper proposes a novel mechanism for forming PBHs at a late epoch (around $z \simeq 10^4$–10^7). Later, we will see whether we want PBHs to make up the entire DM from the cosmological constraint $z \geqslant 10^6$. The key ingredient is a DM fermion that couples to a long-range scalar. Due to the presence of this coupling to matter, the scalar field evolution is controlled by an effective potential $V^{\rm eff}(\phi)$ (Das et al. 2006). Typically, the shape of the effective potential has a minimum, and the scalar field adiabatically follows the minimum (Khoury & Weltman 2004) of the effective potential. The dynamics of scalars with self-interacting potential in such chameleon theories can also give rise to a temporary epoch of early dark energy (EDE) before the CMB (Gogoi et al. 2021; Karwal et al. 2022) and can relax Hubble tension. It has been explicitly shown, for the case of usual dark energy (Afshordi et al. 2005), that such a system of interacting DM–scalar fluid would encounter a perturbative instability when a matter particle turns nonrelativistic. In Gogoi et al. (2021), the same mechanism was extended for EDE theories, and it was shown that even in a radiation-dominated era, the EDE phase would encounter an exponential instability in DM perturbation when it turns nonrelativistic. In our case, the DM mass is of the order of keV—so one would expect the instability to occur around $z_T \simeq 10^6$–10^7.

To find the exact epoch when the fluctuation grows nonlinear, one needs to solve for the linear perturbation equations, evolving it from the Big Bang to a redshift around z_T. We adopt the generalized dark matter (GDM) formalism for our DM–scalar fluid, as done in Hu (1998). In this formalism, the background equation of the fluid is parameterized by its equation of state, $w_{\phi-\psi}$, which we take to be a function of the redshift z. In early times, since the fluid is relativistic, the coupling between the DM and the scalar field could be ignored (as it couples through the trace of the energy-momentum tensor). So, we take $w_{\phi-\psi_1} \sim \frac{1}{3}$ at high redshifts, and as the DM tends to become nonrelativistic around the redshift z_T, the effective coupling turns on. For a quadratic self-interacting scalar potential, the fermion–scalar fluid effectively behaves like EDE for a short duration—soon after, though, the fluid sound speed square c_s^2 turns negative, which results in a strong instability in the fluid perturbation. For details of the evolutions of c_s^2 and $w_{\phi-\psi_1}$, we refer to the works of Gogoi et al. (2021) and Afshordi et al. (2005). It was shown in these works that the DM–scalar fluid perturbation starts to grow exponentially, even in a radiation-dominated era, once the sound speed becomes imaginary. In this work, we show that this mechanism would form a dense early DM halo that finally collapses into a PBH due to cooling through scalar radiation (Flores & Kusenko 2021a).

The perturbation equations for our fluid in synchronous gauge from the GDM formalism are given by Gogoi et al. (2021):

$$\dot{\delta} = -(1+w)\left(\theta + \frac{\dot{h}}{2}\right) - 3(c_s^2 - w)H\delta, \tag{2}$$

$$\dot{\theta} = -(1-3c_s^2)H\theta + \frac{c_s^2 k^2}{1+w}\delta. \tag{3}$$

To solve the background and perturbation equations, we modify the Boltzmann code CLASS (Blas et al. 2011; Lesgourgues 2011), to replace the CDM component with an extra fluid component that describes our fluid through $w_{\phi-\psi}$ and c_s^2. In Figure 1, we indeed see that around z_F the density fluctuations of the ϕ–ψ fluid shoot up

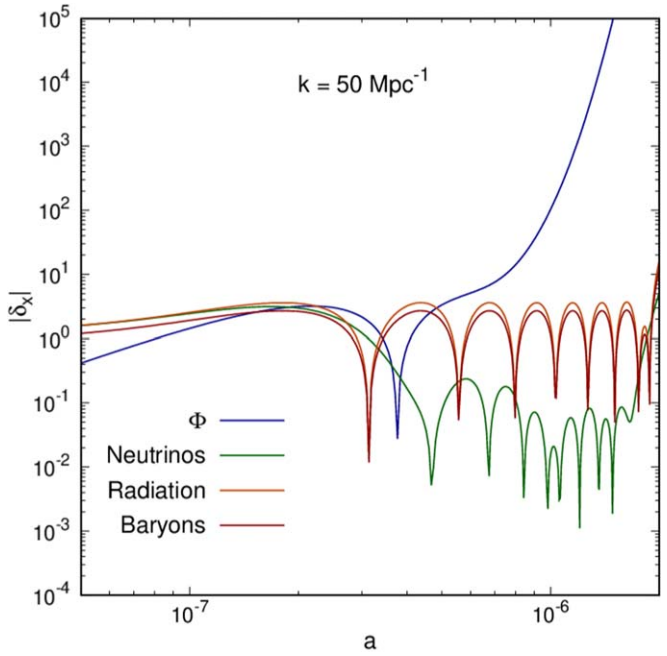

Figure 1. $|\delta|$ vs. scale factor a for a typical wavenumber that is inside the Compton scale of the scalar field around the PBH formation redshift $z_T = 10^6$. We can see that the growth of $|\delta_\Phi|$ is exponential, which makes this mode go nonlinear, then finally collapse to form PBHs.

to huge values compared to those of the other components, such as CDM and the neutrinos from the standard ΛCDM scenario. This exponential growth makes the perturbation turn nonlinear very quickly, followed by the formation of dense early halos, which evolve into PBHs (Flores & Kusenko 2021a) by loose energy through scalar radiation.

There are two main concerns related to the formation of DM PBHs at such a late epoch, a few *e*-foldings prior to the CMB. First of all, one needs to check whether the appearance of DM so late in the universe is at all viable from CMB and structure formation perspectives. From recent studies, it seems that if DM is produced earlier than $z \geqslant 10^6$, one can satisfy both CMB (Sarkar et al. 2017; Agarwal et al. 2015) and large-scale structure (Sarkar et al. 2016; Sarkar et al. 2017) observations, as well as the constraints from local Milky Way satellite observations (Das & Nadler 2021).

The second challenge is that the horizon size around this late redshift is very large, and if one were to produce horizon-size PBHs, the PBH mass would be stupendously large ($M > 10^{11} M_\odot$, known as SLABs, or stupendously large black holes). This will be subject to many constraints arising from dynamical friction and the destruction of galaxies in the cluster $f_{\rm PBH} \lesssim 10^{-3}$ (Carr et al. 2021b). But we will show how the mass of the scalar field in our example is typically much higher than the local Hubble constant. As such, the Compton wavelength or the range of the fifth force is much smaller than the horizon. As an attractive fifth force is the main reason for forming PBHs, one would naturally expect the size of the PBH to be much smaller than the horizon mass at the formation epoch.

During the radiation domination, $H = (2t)^{-1}$, such that the age of the universe t can be related to the temperature of the thermal bath T, as follows:

$$t \approx 2.42\, g_*^{-1/2} \left(\frac{T}{1\ \text{MeV}}\right)^{-2} \text{s}. \tag{4}$$

Using Equations (1) and (4), we find that a PBH being formed at redshift $z_T \simeq 10^6$ is expected to have a horizon size

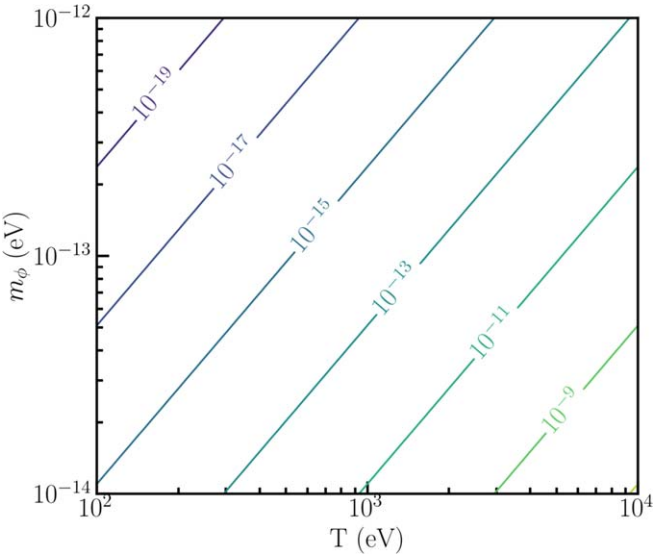

Figure 2. The contours above delineate different PBH masses in solar units as a function of the $T - m_\phi$ parameter space, derived using Equation (5), where T is the temperature of the universe at the epoch of formation of the PBH and m_ϕ is the mass of the scalar field mediating the fifth force.

mass, $M_{\rm BH} \sim 10^{12} M_\odot$, as evaluated from Equation (1), which is much heavier than the mass window mentioned above. But if, as in our case, only a fraction of the horizon mass (enclosed in the Compton volume of the scalar) collapses into the black hole, we find that

$$M_{\rm BH} = \frac{\gamma c^3 t}{G} \approx 2.03 \times 10^5 \gamma \left(\frac{t}{1\ \text{s}}\right) M_\odot \left(\frac{m_\phi}{H}\right)^{-3}, \tag{5}$$

where m_ϕ is the mass of the scalar field. The term $(m_\phi/H)^{-3}$ provides us with an extra parameter for tweaking $M_{\rm BH}$, as can be seen from Figure 2.

We discuss a scenario where the PBHs form at a temperature ∼1 keV in the presence of a scalar field of mass $m_\phi \sim 10^{-13}$ eV, so that the factor $(H/m_\phi)^3$ corresponds to a value $\sim 10^{-25}$. The density of the thermal bath derived as the function of the Hubble parameter, $3H^2 M_{\rm Pl}^2/8\pi$, is evaluated as $\sim 10^{12}\,\text{eV}^4$ during this time period. Assuming a monochromatic mass function, the masses of the PBHs formed can be estimated as the mass enclosed within the Hubble horizon, $M_H \sim (H^{-1})^3 \rho \sim M_{\rm Pl}^2/H$, multiplied by the factor $(H/m_\phi)^3$. With the choice of the parameter space as discussed above, the PBHs are expected to form with mass $M_{\rm BH} \sim 10^{-14} M_\odot$. This mass corresponds to a Schwarzschild radius, $\sim M_{\rm BH}/M_{\rm Pl}^2 \sim 10^{-9}$ cm, far below the distance measures of this study.

3. Static Structure of Primordial Halos

It was pointed out in Flores & Kusenko (2021a) that in the presence of an attractive long-range force mediated by a scalar field, an intermediate state of a DM halo forms, as this attractive "fifth force" is balanced by Fermi pressure. Accelerated DM particles moving in the halo will emit scalar radiation due to the long-range interaction, resulting in the halo losing energy, so that it may collapse rapidly to form a PBH. The dipole radiation due to the coherent motion of the particles should vanish, because the particles are identical, while the higher moments are expected to be negligible. On the other hand, where the radiation is due to particles behaving as incoherent sources, the radiated power depends linearly on the

number of DM particles in the halo. The halo can also lose energy through scalar bremsstrahlung radiation, where the dominating radiation is quadruple, as the DM particles are identical (Maxon & Corman 1967; Maxon 1972). As the halo decreases in size, the collapse timescale increases, the diffusion timescale decreases, and, at some point, the diffusion becomes slower than the collapse. This results in the radiation being trapped, and the cooling occurs from the surface. A DM halo can collapse into a black hole only if the rate of energy loss, $\tau_{\rm loss}$, is less than the expansion rate of the universe, $\sim H^{-1}$.

In this section, we numerically show that, indeed, a temporary static phase is possible where the Fermi degeneracy pressure balances the scalar forces. We solve numerically for the static profile of the ϕ field. We refer to Brouzakis & Tetradis (2006), Lee & Pang (1987), and Chanda & Das (2017) for detailed derivations of these equations. We consider the DM to be a fermion field, ψ, self-interacting through a scalar field, ϕ. We discuss a more general interaction as compared to the original mass-varying neutrino model (Fardon et al. 2004), which considers the Majorana mass term to be a linear function of ϕ. In this analysis, we introduce a function $f(\phi)$ so that the DM mass is obtained as$m_\psi = m_D^2/f(\phi)$, where m_D is the Dirac mass. We choose the self-interaction to have the form $f(\phi) = \lambda_\psi \phi$.

Prior to the phase transition, an effective potential controls the dynamics of ϕ (Fardon et al. 2004):

$$V_{\rm eff} = \rho_\psi + V(\phi). \tag{6}$$

In our analysis, we use $V(\phi) = m_\phi^2 \phi^2$, where m_ϕ is the scalar field mass.

We assume the DM particles to be weakly interacting and nonscattering, such that the motion of the ψ particles can be determined using the Thomas–Fermi approximation (Brouzakis & Tetradis 2006); that is, the physical parameters, such as density, pressure, and number density, are characterized by the distribution $\sim[1 + \exp(\epsilon_F/T)]^{-1}$, where the Fermi energy $\epsilon_F = \sqrt{p_F^2 + m_\psi^2}$, with p_F being the Fermi momentum. We consider a simpler scenario by doing the calculations in the zero temperature limit (Brouzakis & Tetradis 2006), and we derive an explicit form of the trace of the energy-momentum tensor, $T^\mu_\mu = \rho - 3p$,

$$T^\mu_\mu = \frac{m_\psi^2}{2\pi^2}\left(p_F\sqrt{p_F^2 + m_\psi^2} - m_\psi^2 \ln\left(\frac{p_F + \sqrt{p_F^2 + m_\psi^2}}{m_\psi}\right)\right), \tag{7}$$

and the pressure,

$$p = \frac{m_\psi^2}{8\pi^2}\left[\frac{2p_F^3}{3m_\psi^2}\sqrt{p_F^2 + m_\psi^2} - \left(p_F\epsilon_F - m_\psi^2 \ln\left(\frac{p_F + \epsilon_F}{m_\psi}\right)\right)\right], \tag{8}$$

where $\epsilon_F = \sqrt{p_F^2 + m_{\psi_1}^2}$.

In the weak limit of general relativity, the Klein–Gordon equation can be written as

$$\phi'' + \frac{2}{r}\phi' = \frac{dV(\phi)}{d\phi} - \frac{d\ln[m_\psi]}{d\phi}T^\mu_\mu, \tag{9}$$

and the Euler equation for pressure, p, as

$$\frac{dp}{d\phi} = \frac{d[\ln m_\psi]}{d\phi}T^\mu_\mu. \tag{10}$$

We obtain a static solution for ϕ, as demonstrated in Figure 3, which is determined by how the attractive fifth force is balanced by the local Fermi pressure, as derived from the Euler equation, (10), and the Klein–Gordon equation, (9). The mass enclosed in the DM halo corresponds to a Schwarzschild radius of $\sim 10^{-9}$ cm, which is much smaller than the size of the halo. The density at the core of the profile can be predicted without explicitly carrying out the numerical calculations. Because of the self-interactions through the ϕ field, the density of the DM particles near the core of the profile should be much denser, by a factor of $(m_\phi/H)^3$. Therefore, for PBHs formed at $\sim$1 keV for DM particles self-interacting through a scalar of mass $m_\phi \sim 10^{-13}$ eV, the core density should be $\sim 10^{12}$ eV$^4 (m_\phi/H)^3 \sim 10^{37}$ eV^4, which agrees very well with the results from the numerical studies. We should remind ourselves from the earlier calculations that, at $\sim$1 keV, the factor $(m_\phi/H)^3 \sim 10^{25}$, for the given scalar mass, and the factor 10^{12} eV^4 is the density of the thermal bath evaluated at the same temperature.

4. PBH Mass Function and PBH DM Abundance

In this section, we focus on estimating the DM abundance of PBHs from the collapse of primordial fluctuations in the radiation-dominated era. Though we mostly concentrate on the cosmology with the exponential growth of the perturbation prior to the phase transition, our treatment and numerical code as developed in this section remain generic and can be applied to calculate PBH abundances with different perturbation growth rates. It is instructive to note here that, in this work, we consider a nonmonochromatic mass function, i.e., the mass of a PBH formed from collapse does not necessarily have to be equal to the horizon mass.

The mass distribution of a PBH is usually stated in terms of $f(M)$, the fraction of CDM made up of PBHs of a given mass M, which is given by Byrnes et al. (2018):

$$f(M) = \frac{1}{\Omega_{\rm CDM}}\frac{d\Omega_{\rm PBH}}{d\ln M}, \tag{11}$$

where $\Omega_{\rm CDM}$ and $\Omega_{\rm PBH}$ are the abundances of the CDM and PBH, respectively.

Using the Press–Schechter formalism (Press & Schechter 1974), and taking into account the mass fraction of the universe that collapses to form PBHs at the time of formation, we can write the expression for $\beta(M)$ as

$$\beta(M) = 2\int_{\delta_c}^{\infty}\frac{M}{M_h}Pr(\delta)\,d\delta, \tag{12}$$

where δ_c is the critical value of δ at the time of the horizon entry for the PBH formation and $Pr(\delta)$ is the probability density function of the density contrast. Assuming a Gaussian distribution of density fluctuations, $Pr(\delta)$ can be given as

$$Pr(\delta) = \frac{1}{\sqrt{2\pi\sigma^2(R)}}\exp\left(-\frac{\delta^2}{2\sigma^2(R)}\right), \tag{13}$$

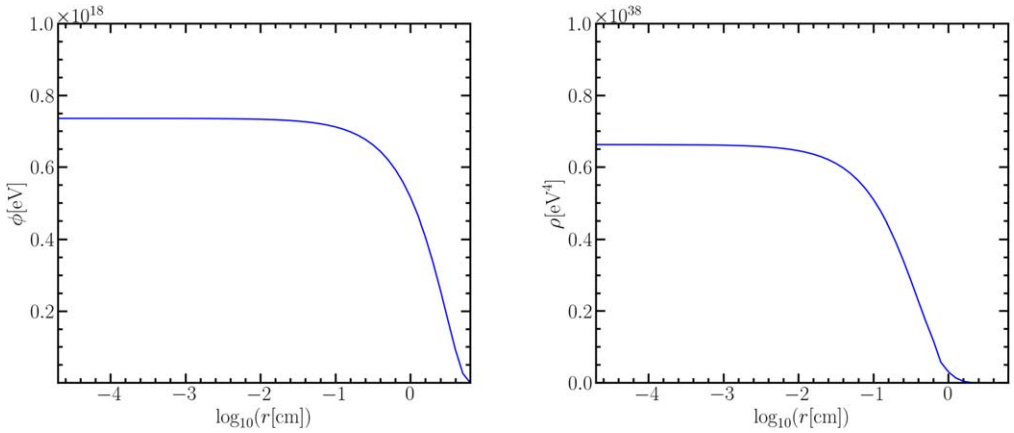

Figure 3. In the above, we demonstrate the static profile, which is obtained by solving Equations (10) and (9). The left plot shows the static profile for the scalar field ϕ, and the right plot delineates the density profile, ρ, of the resulting DM halo. As discussed in the main text, this halo may later collapse due to cooling through scalar radiation, and eventually form a PBH (Flores & Kusenko 2021a).

where $\sigma(R)$ is the smoothed density fluctuations over a smoothing radius R, which can be given as

$$\sigma^2(R) = \int_0^\infty \frac{dk}{k}\Delta(k)W_R^2(k), \tag{14}$$

where $W_R^2(k)$ is the window function of the smoothing radius R, which we take as a step function, and which is given by

$$W_R(k) = \theta\left(\frac{1}{R} - k\right). \tag{15}$$

The smoothing radius R can be related to the horizon mass M_h using the following relation (see Appendix A.1):

$$\frac{1}{R} = \frac{k_B T_0}{2}\left(\frac{g_{*,s}(T_0)}{g_{*,s}(T_h)}\right)^{1/3}\left(\frac{g_{*,\rho}(T_h)}{45\hbar^3c^3\pi G}\right)^{1/4}\frac{1}{\sqrt{M_h}}. \tag{16}$$

The dimensionless power spectra $\Delta(k)$ in Equation (14) can be written as

$$\Delta(k, z) = \frac{k^3P(k, z)}{2\pi^2} = A_s\delta^2(k, z), \tag{17}$$

where $P(k)$ is the density power spectra and A_s is the primordial power spectrum amplitude.

Now, considering the formation of PBHs from the gravitational collapse of primordial density fluctuations in the radiation-dominated phase of the early universe as a critical phenomenon, we can write the following equation for the PBH mass at its formation (Choptuik 1993):

$$M = KM_h(\delta - \delta_c)^\gamma, \tag{18}$$

where M is the mass of the PBH, δ is the density contrast, δ_c is the critical value of δ at the time of horizon entry, M_h is the horizon mass at the time when the fluctuations entered the horizon, and K and γ are constants that depend on the shape of the fluctuations and the background equation of state, respectively.

The above equation can be inverted to give δ as a function of M:

$$\delta = \left(\frac{M}{KM_h}\right)^{1/\gamma} + \delta_c = \mu^{1/\gamma} + \delta_c. \tag{19}$$

where $\mu = M/(KM_h)$. Now, using Equations (11), (12), and (19), we can write $f(M)$ as (Byrnes et al. 2018)

$$f(M) = \frac{2}{\Omega_{\rm CDM}}\int_{-\infty}^{\infty} Pr(M_h)\frac{M}{\gamma M_h}\mu^{1/\gamma}\left(\frac{M_{\rm eq}}{M_h}\right)^{1/2} d\ln M_h, \tag{20}$$

where $Pr(M_h)$ is the probability density function of the density contrast in terms of M_h,

$$Pr(M_h) = \frac{1}{\sqrt{2\pi\sigma^2(M_h)}}\exp\left(-\frac{(\delta_c + \mu^{1/\gamma})^2}{2\sigma^2(M_h)}\right). \tag{21}$$

4.1. Power Spectrum P(k) for Exponentially Growing δ

In this section, we discuss the case where the density contrast grows exponentially, i.e., $\delta \propto \exp(\lambda k c_s t)$, where c_s is the sound speed and λ is a constant that has been tuned to a suitable value, such that the formed PBH fractional abundances $f(M)$ are within 1. In this case, where the scaling (the exponential growth) regime starts from $z_{\rm in}$ and lasts until redshift z_T, the power spectrum can be written as

$$P(k, z) = \begin{cases} \frac{2\pi^2A_s}{k^3} & \text{if } k \leqslant k(z_T), \\ \frac{2\pi^2A_s}{k^3}\exp\left(\frac{2\,c_m}{(1+z_T)^2}\right)\exp\left(-\frac{2\,c_m}{(1+z(k))^2}\right) & \text{if } k(z_T) < k \leqslant k(z_{\rm in}), \\ \frac{2\pi^2A_s}{k^3}\exp\left(\frac{2\,c_m}{(1+z_T)^2}\right)\exp\left(-\frac{2\,c_m}{(1+z_{\rm in})^2}\right)\left(\frac{\log(1+z_{\rm in})}{\log(1+z(k))}\right)^2 & \text{if } k > k(z_{\rm in}) \end{cases} \tag{22}$$

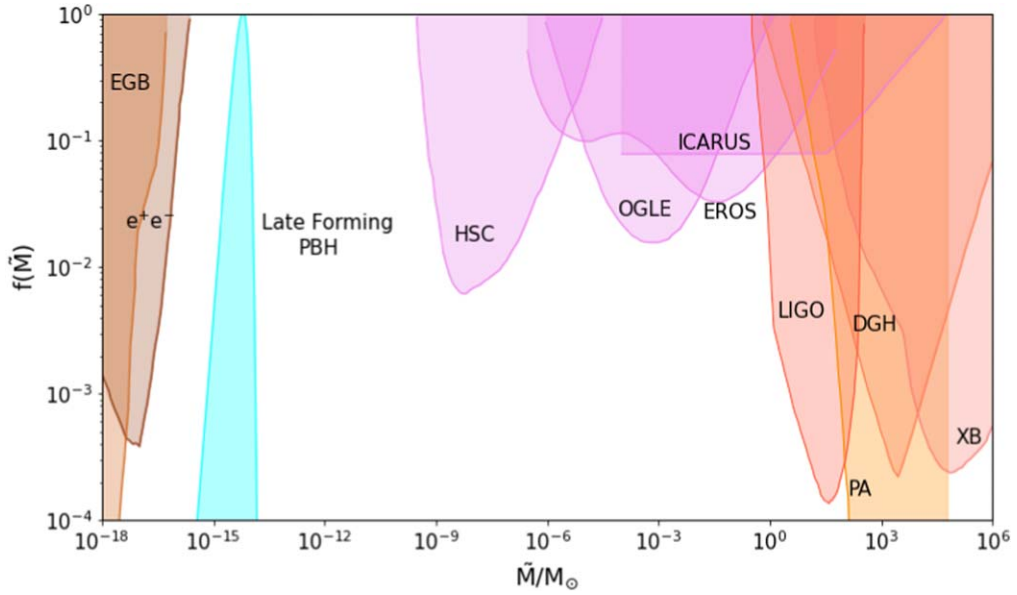

Figure 4. The plot of the late-forming PBH mass function, $f(\tilde{M})$, shown in cyan, suggests that the PBH density can be attributed to the entire DM density in the universe. The PBH mass function shown in this figure is for $f_{\max}(\tilde{M}) = 1$ (ie., $f_{\rm PBH} \approx 1$), for a redshift of formation $z_T \sim 10^6$.

where $c_m = \lambda k c_s / 2\sqrt{\Omega_{r,0}} H_0$ and z as a function of k can be given as (see Appendix A.2)

$$1 + z(k) = \frac{k}{k_B T_0}\left(\frac{g_{*,s}(T_0)}{g_{*,s}(T_h)}\right)^{-1/3} \times g_{*,\rho}^{-1/4}(T_h)\left(\frac{4\pi^3 H_0^2\, G\, \Omega_{r,0}}{45\,\hbar^3 c^9}\right)^{-1/4}, \quad (23)$$

where $k(z_T)$ and $k(z_{\rm in})$ are different wavenumbers that have just entered the horizon corresponding to their respective redshifts and $z_{\rm in}$ is the redshift at which this growth starts, ending at redshift z_T. In Equation (22), the first case ($k \leqslant k(z_T)$) represents the scales that are still outside the horizon at redshift z_T, the second case ($k(z_T) < k \leqslant k(z_{\rm in})$) represents the scales that entered during the exponential growth period, and the last case ($k > k(z_{\rm in})$) represents the scales that entered before the growth period and grew logarithmically in the initial phase, following the standard ΛCDM cosmology–driven growth. After that, all the scales grow by equal amounts in the exponentially growing regime. For our calculation, we have taken $z_{\rm in} = 3 \times 10^7$. We cut the power spectrum for $k > k(z_{\rm in})$, as these modes enter the horizon before the exponential growth regime starts.

4.2. Results

We compute the PBH mass function $f(M)$ using Equations (20) and (21), where, for $\sigma(M_h)$, we use Equations (14), (16), and (22). For our calculation, we use $K = 11.9$, $\gamma = 0.37$, as suggested by Green & Liddle (1999), and $\delta_c = 2.07$ from Savastano et al. (2019). The corresponding plots are shown in Figure 4. In this figure, all the constraint plots are taken from Flores & Kusenko (2021a). For this calculation, we have not taken the whole horizon to be under the influence of the exponential growth, but rather we have taken a small fraction of it, which is basically the ratio between the range of the scalar field, i.e., the Compton scale and the Hubble radius ($(m_\phi/H)^{-1}$). This is taken into account in the calculation as a factor of $(m_\phi/H)^{-3} \sim 10^{-25}$ in the black hole mass. Also, since the Compton scale is smaller than the horizon scale, at any epoch, there will be multiple numbers of Compton patches that will contribute to the formation of PBHs. We have incorporated this into the calculation by multiplying a factor of $(m_\phi/H)^3 \sim 10^{25}$ in the expression for $f(M)$ in Equation (20). Therefore, the modified expression becomes

$$f(\tilde{M}) = \left(\frac{m_\phi}{H}\right)^3 \frac{2}{\Omega_{\rm CDM}} \int_{-\infty}^{\infty} \times Pr(M_h) \frac{\tilde{M}}{\gamma M_h} \tilde{\mu}^{1/\gamma} \left(\frac{M_{\rm eq}}{M_h}\right)^{1/2} d\ln M_h, \quad (24)$$

where $\tilde{M} = M\left(\frac{m_\phi}{H}\right)^{-3}$, which is defined as the actual black hole mass when a Compton range of collapse is considered, and $\tilde{\mu} = \tilde{M}/(KM_h)$. One can think of this treatment as being analogous to the modified definition of β for the nonmonochromatic mass function, given in Equation (12), as opposed to the Press–Schechter theory, where the factor of M/M_h in β never appears, due to assumption of the monochromatic mass function. Also, hypothetically, one can think of the constant Compton scale as our effective horizon. There is a sharp exponential growth in the power spectrum inside this effective horizon, and it reflects an approximate sharp peak in $f(\tilde{M})$, which we have got in our plot.

The plot in Figure 4 shows a peak $f(\tilde{M})$ for a certain PBH mass, where the PBHs contribute the total DM density in the universe. Since the Compton scale remains constant with time, the ratio between the Compton scale and the Hubble radius ($(m_\phi/H)^{-1}$) decreases with time. This ratio takes its highest value in our calculation at the beginning of the growth regime. For this reason, $f(\tilde{M})$ gets the highest contribution from the PBH mass corresponding to this scale. We find that, given enough span for the exponential growth regime ($z_T \sim 10^6$), our model can give $f_{\max}(\tilde{M}) = 1$, which is a good approximation to $f_{\rm PBH} = 1$, suggesting that these PBHs can make up all the DM in this case. Increasing the termination redshift of the

growth regime, z_T, beyond $\sim 10^6$, decreases the abundance of the PBHs, and hence the corresponding $f_{\rm PBH}$ goes below 1.

5. Conclusions and Discussion

In this paper, we present a novel mechanism for late-forming ($z_T \sim 10^6$) PBHs. Keeping the scale-invariant inflationary primordial power as it is, we show here that a late-phase transition in a fermion–scalar fluid can produce DM PBHs, due to the formation of an early dense halo in the radiation-dominated era, which evolves into PBHs by cooling though scalar radiation. We also perform a detailed analytical calculation of the PBH mass function for these cases and show that, in principle, these PBHs can even constitute almost all of the DM. The PBH masses in these models are in the range of $\sim 10^{-16}$–$10^{-14} M_\odot$.

In the standard ΛCDM cosmology, with the growth function being logarithmic in the radiation-dominated era, gravity alone cannot clump the matter that collapses into PBHs. In this work, we have considered a scenario where the growth rate of the primordial inhomogeneities is exponential. This can occur in a scenario where a force stronger than gravity emerges, due to the interaction between an additional scalar field and a fermionic particle beyond the standard model. The exponential growth of the perturbations occurs when the fermionic particles become nonrelativistic at around $z \sim 10^6$. This can lead to the formation of numerous low-mass DM halos, which can further collapse due to scalar radiation and form PBHs of similar masses. We also perform a detailed calculation of the PBH mass function for this model. Though Flores & Kusenko (2021a) have also worked out the PBH fraction for a similar PBH formation mechanism (albeit in the context of a different model), an approximate estimation using the Press–Schechter theory was used there. In this paper, we have presented a detailed and thorough calculation of $f(M)$ for the first time, given our knowledge of early DM halo formation.

There is an allowed mass range for PBHs of around 10^{-16}–$10^{-10} M_\odot$ (the sublunar-mass range), where the constraints on $f_{\rm PBH}$ are almost nonexistent. Though this mass range was previously constrained due to femtolensing, optical microlensing, white-dwarf survival, and neutron star capture, it is no longer constrained in the light of recent studies (Katz et al. 2018; Montero-Camacho et al. 2019). Our model allows the formation of PBHs in this window for a keV mass fermion and with other viable model parameters—therefore, these PBHs can constitute all the DM. In principle, we should use nonmonochromatic constraints (Carr et al. 2017) to compare with our $f(M)$, but since our $f(M)$ turns out to be very narrow (if we approximate our $f(M)$ with a log-normal distribution, the corresponding σ would be $\lesssim 0.2$), in which case monochromatic constraints will be a good approximation to the nonmonochromatic constraints derived using the method provided by Carr et al. (2017; e.g., the nonmonochromatic constraints given for the log-normal distribution $\sigma = 2$ case in Figure 20 of Carr et al. 2021a).

These PBHs are not expected to evaporate or even to accrete mass significantly in a Hubble timescale (Rice & Zhang 2017; Pandey & Mangalam 2018), which makes them very good candidates for DM. Though some works considering the capture of PBHs by white dwarfs and neutron stars have suggested strong bounds on sublunar-mass PBHs (Pani & Loeb 2014), other recent studies (Defillon et al. 2014) have disputed these bounds, on the grounds of the recent understanding of DM density in globular clusters, which is now known to be much lower than assumed in these analyses (Ibata et al. 2013). Though the constraints on PBHs are the subject of a rapidly evolving field of research, meaning that the current PBH abundance constraints over various mass windows should be taken as order-of-magnitude estimates, more detailed future studies will be able to put more robust bounds around this mass window.

Also, in our model, the PBHs form through the scalar radiation of dense halos, which are just clumps of matter and have a distribution of initial angular momentum. As a result, these PBHs would have considerable spin, which, in principle, will be able to be detected through future gravitational-wave observations (Flores & Kusenko 2021b).

We are grateful to Alexander Kusenko for his encouraging and valuable comments on the manuscript. We also thank Yacine Ali Haimoud for reading the manuscript and giving his valuable suggestions. S.D. and K.P. acknowledge SERB, India grant CRG/2019/006147 for supporting this project. We would like to thank the ICTS LTPDM workshop on PBHs, where a few talks and discussions helped in shaping this work in its initial stages.

Appendix
Details of Derivations

A.1. Relation between Smoothing Radius R *and Halo Mass* M_h*: Equation (16)*

Using Friedmann's equation, $H^2 = 8\pi G\rho/3c^2$, we can write the energy density ρ as

$$\rho = \frac{\pi^2 g_{*,\rho}(T)}{30\hbar^3 c^3}(k_B T)^4, \tag{A1}$$

where $k = aH/c$ and the scale factor a, in terms of the temperature T of the thermal bath, is

$$a = \left(\frac{g_{*,s}(T_0)}{g_{*,s}(T)}\right)^{1/3}\frac{T_0}{T}, \tag{A2}$$

where T_0 is the temperature at $a = 1$. The horizon mass can now be obtained by

$$M_h = \frac{4}{3}\pi\left(\frac{c}{H}\right)^3\frac{\rho}{c^2} = \frac{4\pi c}{3}\frac{\rho}{H^3}, \tag{A3}$$

from Equation (A3), and by using Friedmann's equation we get

$$H = \frac{c^3}{2GM_h}. \tag{A4}$$

Now, using Equations (A1) and (A4), we get

$$M_h = \left(\frac{45\hbar^3 c^{11}}{16\pi^3 G^3 k_B^4}\right)^{1/2}\left(\frac{1}{g_{*,\rho}(T_h)}\right)^{1/2}\frac{1}{T_h^2}. \tag{A5}$$

Here, T_h is the temperature corresponding to the horizon mass M_h, since we know that the length x corresponding to the wavenumber k can be written as $1/R = aH/(2\pi c)$. Now, using

Equations (A2), (A4), and (A5), we get

$$\frac{1}{R} = \left(\frac{k_B T_0}{2}\right)\left(\frac{g_{*,s}(T_0)}{g_{*,s}(T_h)}\right)^{1/3}\left(\frac{g_{*,\rho}(T_h)}{45\pi G\hbar^3 c^3}\right)^{1/4}\frac{1}{\sqrt{M_h}}. \quad \text{(A6)}$$

A.2. Relation between Wavenumber k and Redshift z: Equation (23)

In the radiation-dominated era, $H = 1/(2t)$ and $a = (4\Omega_{r,0}H_0^2)^{1/4}\sqrt{t}$. Now, using $k = \frac{2\pi}{R}$ and Equations (A4) and (A6), we finally get

$$k = (k_B T_0)\left(\frac{g_{*,s}(T_0)}{g_{*,s}(T_h)}\right)^{1/3} \times (g_{*,\rho}(T_h))^{1/4}\left(\frac{4\pi^3 H_0^2\, G\, \Omega_{r,0}}{45\,\hbar^3 c^9}\right)^{1/4}(1+z), \quad \text{(A7)}$$

where $1 + z(k)$ can also be written as

$$1 + z(k) = \frac{k}{k_B T_0}\left(\frac{g_{*,s}(T_0)}{g_{*,s}(T_h)}\right)^{-1/3} \times g_{*,\rho}^{-1/4}(T_h)\left(\frac{4\pi^3 H_0^2\, G\, \Omega_{r,0}}{45\,\hbar^3 c^9}\right)^{-1/4}. \quad \text{(A8)}$$

ORCID iDs

Kanhaiya Lal Pandey https://orcid.org/0000-0003-3536-1730
Subinoy Das https://orcid.org/0000-0002-7771-180X

References

Afshordi, N., Zaldarriaga, M., & Kohri, K. 2005, PhRvD, 72, 065024
Agarwal, S., Corasaniti, P. S., Das, S., & Rasera, Y. 2015, PhRvD, 92, 063502
Ashoorioon, A., Casadio, R., Cicoli, M., Geshnizjani, G., & Kim, H. J. 2018, JHEP, 2018, 172
Ashoorioon, A., Rostami, A., & Firouzjaee, J. T. 2021, JHEP, 2021, 087
Baker, M. J., Breitbach, M., Kopp, J., & Mittnacht, L. 2021, arXiv:2105.07481
Ballesteros, G., & Taoso, M. 2018, PhRvD, 97, 023501
Bhattacharya, S., Das, A., & Dutta, K. 2021, JCAP, 2021, 071
Bird, S., Cholis, I., Muñoz, J. B., et al. 2016, PhRvL, 116, 201301
Blas, D., Lesgourgues, J., & Tram, T. 2011, JCAP, 2011, 034
Brouzakis, N., & Tetradis, N. 2006, JCAP, 01, 004
Byrnes, C. T., Hindmarsh, M., Young, S., & Hawkins, M. R. 2018, JCAP, 2018, 041
Cappelluti, N., Hasinger, G., & Natarajan, P. 2022, ApJ, 926, 205
Carr, B., Kohri, K., Sendouda, Y., & Yokoyama, J. 2021a, RPPh, 84, 116902
Carr, B., & Kühnel, F. 2020, ARNPS, 70, 355
Carr, B., Kühnel, F., & Visinelli, L. 2021b, MNRAS, 501, 2029
Carr, B., Raidal, M., Tenkanen, T., Vaskonen, V., & Veermäe, H. 2017, PhRvD, 96, 023514
Carr, B. J., & Lidsey, J. E. 1993, PhRvD, 48, 543
Chanda, P. K., & Das, S. 2017, PhRvD, 95, 083008
Choptuik, M. W. 1993, PhRvL, 70, 9
Clesse, S., & García-Bellido, J. 2015, PhRvD, 92, 023524
Cotner, E., & Kusenko, A. 2017a, PhRvL, 119, 031103
Cotner, E., & Kusenko, A. 2017b, PhRvD, 96, 103002
Cotner, E., Kusenko, A., Sasaki, M., & Takhistov, V. 2019, JCAP, 2019, 077
Cotner, E., Kusenko, A., & Takhistov, V. 2018, PhRvD, 98, 083513
Crawford, M., & Schramm, D. N. 1982, Natur, 298, 538
Das, S., Corasaniti, P. S., & Khoury, J. 2006, PhRvD, 73, 083509
Das, S., Maharana, A., & Muia, F. 2021, arXiv:2112.11486
Das, S., & Nadler, E. O. 2021, PhRvD, 103, 043517
Dasgupta, B., Laha, R., & Ray, A. 2020, PhRvL, 125, 101101
Defillon, G., Granet, E., Tinyakov, P., & Tytgat, M. H. G. 2014, PhRvD, 90, 103522
Ezquiaga, J. M., García-Bellido, J., & Ruiz Morales, E. 2018, PhLB, 776, 345
Fardon, R., Nelson, A. E., & Weiner, N. 2004, JCAP, 10, 005
Flores, M. M., & Kusenko, A. 2021a, PhRvL, 126, 041101
Flores, M. M., & Kusenko, A. 2021b, PhRvD, 104, 063008
Franciolini, G., Kehagias, A., Matarrese, S., & Riotto, A. 2018, JCAP, 2018, 016
García-Bellido, J., Linde, A., & Wands, D. 1996, PhRvD, 54, 6040
García-Bellido, J., & Ruiz Morales, E. 2017, PDU, 18, 47
Gogoi, A., Sharma, R. K., Chanda, P., & Das, S. 2021, AJ, 915, 132
Green, A. M., & Liddle, A. R. 1999, PhRvD, 60, 063509
Gross, C., Landini, G., Strumia, A., & Teresi, D. 2021, JHEP, 2021, 033
Hawking, S. 1971, MNRAS, 152, 75
Hawking, S. W. 1974, Natur, 248, 30
Hawking, S. W. 1975, CMaPh, 43, 199
Hawking, S. W., Moss, I. G., & Stewart, J. M. 1982, PhRvD, 26, 2681
Hindmarsh, M., & Philipsen, O. 2005, PhRvD, 71, 087302
Hu, W. 1998, ApJ, 506, 485
Hütsi, G., Raidal, M., Vaskonen, V., & Veermäe, H. 2021, JCAP, 2021, 068
Ibata, R., Nipoti, C., Sollima, A., et al. 2013, MNRAS, 428, 3648
Ivanov, P., Naselsky, P., & Novikov, I. 1994, PhRvD, 50, 7173
Jedamzik, K. 1997, PhRvD, 55, R5871
Jedamzik, K. 1998, PhR, 307, 155
Kannike, K., Marzola, L., Raidal, M., & Veermäe, H. 2017, JCAP, 2017, 020
Kapadia, S. J., Lal Pandey, K., Suyama, T., Kandhasamy, S., & Ajith, P. 2021, ApJL, 910, L4
Kapadia, S. J., Pandey, K. L., Suyama, T., & Ajith, P. 2020, PhRvD, 101, 123535
Karwal, T., Raveri, M., Jain, B., Khoury, J., & Trodden, M. 2022, PhRvD, 105, 063535
Katz, A., Kopp, J., Sibiryakov, S., & Xue, W. 2018, JCAP, 2018, 005
Kawana, K., & Xie, K.-P. 2022, PhLB, 824, 136791
Khoury, J., & Weltman, A. 2004, PhRvL, 93, 171104
Kodama, H., Sasaki, M., & Sato, K. 1982, PThPh, 68, 1979
Konoplich, R. V., Rubin, S. G., Sakharov, A. S., & Khlopov, M. Y. 1998, AstL, 24, 413
Konoplich, R. V., Rubin, S. G., Sakharov, A. S., & Khlopov, M. Y. 1999, PAN, 62, 1593
Kusenko, A., Sasaki, M., Sugiyama, S., et al. 2020, PhRvL, 125, 181304
La, D., & Steinhardt, P. 1989, PhLB, 220, 375
Laha, R. 2019, PhRvL, 123, 251101
Laha, R., Muñoz, J. B., & Slatyer, T. R. 2020, PhRvD, 101, 123514
Lee, T. D., & Pang, Y. 1987, PhRvD, 35, 3678
Lesgourgues, J. 2011, arXiv:1104.2932
Maxon, M. S., & Corman, E. G. 1967, PhRv, 163, 156
Maxon, S. 1972, PhRvA, 5, 1630
Montero-Camacho, P., Fang, X., Vasquez, G., Silva, M., & Hirata, C. M. 2019, JCAP, 2019, 031
Moss, I. G. 1994, PhRvD, 50, 676
Pandey, K. L., & Mangalam, A. 2018, JApA, 39, 9
Pani, P., & Loeb, A. 2014, JCAP, 2014, 026
Press, W. H., & Schechter, P. 1974, ApJ, 187, 425
Pi, S., Zhang, Y.-l., Huang, Q.-G., & Sasaki, M. 2018, JCAP, 2018, 042
Rice, J. R., & Zhang, B. 2017, JHEAp, 13, 22
Sarkar, A., Mondal, R., Das, S., et al. 2016, JCAP, 04, 012
Sarkar, A., Sethi, S. K., & Das, S. 2017, JCAP, 07, 012
Sasaki, M., Suyama, T., Tanaka, T., & Yokoyama, S. 2016, PhRvL, 117, 061101
Sasaki, M., Suyama, T., Tanaka, T., & Yokoyama, S. 2018, CQGra, 35, 063001
Savastano, S., Amendola, L., Rubio, J., & Wetterich, C. 2019, PhRvD, 100, 083518
Widerin, P., & Schmid, C. 1998, arXiv:astro-ph/9808142
Zel'dovich, Y. B., & Novikov, I. D. 1967, SvA, 10, 602